The Astrophysical Journal, 783:105 (11pp), 2014 March 10 doi:10.1088/0004-637X/783/2/105

EVIDENCE FOR LARGE TEMPERATURE FLUCTUATIONS IN QUASAR ACCRETION DISKS FROM SPECTRAL VARIABILITY

John J. Ruan[1], Scott F. Anderson[1], Jason Dexter[2], and Eric Agol[1]
[1] Department of Astronomy, University of Washington, Box 351580, Seattle, WA 98195, USA; jruan@astro.washington.edu
[2] Departments of Physics and Astronomy, University of California, Berkeley, CA 94720, USA
Received 2013 October 14; accepted 2013 December 27; published 2014 February 21

ABSTRACT

The well-known bluer-when-brighter trend observed in quasar variability is a signature of the complex processes in the accretion disk and can be a probe of the quasar variability mechanism. Using a sample of 604 variable quasars with repeat spectra in the Sloan Digital Sky Survey-I/II (SDSS), we construct difference spectra to investigate the physical causes of this bluer-when-brighter trend. The continuum of our composite difference spectrum is well fit by a power law, with a spectral index in excellent agreement with previous results. We measure the spectral variability relative to the underlying spectra of the quasars, which is independent of any extinction, and compare to model predictions. We show that our SDSS spectral variability results cannot be produced by global accretion rate fluctuations in a thin disk alone. However, we find that a simple model of an inhomogeneous disk with localized temperature fluctuations will produce power-law spectral variability over optical wavelengths. We show that the inhomogeneous disk will provide good fits to our observed spectral variability if the disk has large temperature fluctuations in many independently varying zones, in excellent agreement with independent constraints from quasar microlensing disk sizes, their strong UV spectral continuum, and single-band variability amplitudes. Our results provide an independent constraint on quasar variability models and add to the mounting evidence that quasar accretion disks have large localized temperature fluctuations.

Key word: quasars: general

Online-only material: color figures

1. INTRODUCTION

A well-known characteristic of the quasar phenomena is their strong flux variability in many wavelength regimes, including the radio, optical, X-ray, and γ-rays (Ulrich et al. 1997). In particular, the rise of optical large-scale time-domain imaging surveys has led to many recent investigations of broadband quasar optical variability properties using large numbers of well-sampled light curves, especially for use in quasar selection (Kelly et al. 2009; Kozłowski et al. 2010; MacLeod et al. 2010, 2011; Schmidt et al. 2010; Butler & Bloom 2011; Kim et al. 2011; Ruan et al. 2012; Andrae et al. 2013; Zu et al. 2013). These studies have generally revealed that quasars are stochastically variable on the $\sim$10%–20% level in flux on long timescales and show weaker, correlated variability on timescales $\lesssim$1 yr in the rest frame. The physical cause of quasar variability is still unclear, but since the optical continuum is likely to be dominated by emission from the accretion disk, some studies have suggested that changes in the global accretion rate in the disk may be able to produce such effects (Pereyra et al. 2006; Li & Cao 2008; Zuo et al. 2012). These claims appear to be supported (although not implied) by various observed trends between optical variability amplitude, black hole mass, and luminosity in different quasars (Hook et al. 1994; Garcia et al. 1999; Vanden Berk et al. 2004; Wilhite et al. 2008; Bauer et al. 2009; Kelly et al. 2009; MacLeod et al. 2010; Zuo et al. 2012), in turn suggesting that the differences in variability across a sample of quasars may be driven at least in part by their Eddington ratio.

Accretion rate fluctuations are expected in individual quasars due to processes in the disk such as the magnetorotational instability (MRI; Balbus & Hawley 1991), which is now generally accepted to operate in a wide range of accretion flows. Results from non-radiative global simulations of thin magnetized disks have also shown that such accretion flows are almost certain to be highly turbulent (e.g., Armitage et al. 2001; Armitage & Reynolds 2003; Noble et al. 2009; Noble & Krolik 2009; Penna et al. 2010), but the exact characteristics of an MRI flow in a global radiative MHD simulation are currently unclear, especially their stability in the radiation-pressure-dominated regime (see discussions in Hirose et al. 2009; Janiuk & Misra 2012; Jiang et al. 2013). Localized temperature fluctuations in highly turbulent disks will also cause flux variations, and such a scenario may be expected since quasar accretion disks are too large to vary coherently in flux over the short variability timescales observed. The characteristic timescales of quasar flux variability have also been shown to be consistent with the thermal timescale (Kelly et al. 2009), independently motivating accretion disk models involving localized temperature fluctuations. Furthermore, it has been shown that such models of inhomogeneous accretion disks can also simultaneously explain quasar microlensing disk sizes, their strong UV spectral continuum, and single-band optical variability properties (Dexter & Agol 2011).

Although the relative roles of global accretion rate fluctuations and localized temperature fluctuations in accounting for the observed flux variability are unclear, an additional probe is provided by the characteristic bluer-when-brighter trend observed in studies of quasar spectral variability (Cutri et al. 1985; Giveon et al. 1999; Trèvese et al. 2001; Trèvese & Vagnetti 2002; Vanden Berk et al. 2004; Wilhite et al. 2005; Meusinger et al. 2011; Sakata et al. 2011; Schmidt et al. 2012; Meusinger & Weiss 2013). This trend is almost certainly a direct consequence of the underlying quasar variability mechanism and

thus provides an independent test of quasar variability models. Indeed, both global accretion rate changes and localized temperature fluctuations in accretion disks will generically produce bluer-when-brighter trends, but the details of the predicted trend are dependent on the details of the model. Intriguingly, previous investigations of quasar spectral variability have sometimes resulted in disparate conclusions.

Wilhite et al. (2005) used a sample of 315 pairs of repeat spectra of variable quasars from the Sloan Digital Sky Survey (SDSS; York et al. 2000) and constructed "difference spectra" by taking the spectrum of each quasar at the higher-flux epoch and subtracting the spectrum at the lower-flux epoch; this effectively isolates the variable part of the spectrum. After applying a wavelength-dependent spectrophotometric recalibration on each pair of repeat spectra, they find that the resulting composite quasar difference spectrum has a steeper power-law index than the composite of the individual spectra, showing that quasars are indeed bluer when brighter. Based on the composite difference spectrum from that study, Pereyra et al. (2006) fitted synthetic difference spectra generated from a simple Shakura–Sunayev thin-disk model (Shakura & Sunyaev 1973) and showed that the composite difference spectrum can be produced from a simple thin disk in which the global accretion rate has changed (also see Sakata et al. 2011).

In contrast, Schmidt et al. (2012) used a sample of 9093 multi-band quasar light curves from SDSS Stripe 82 to study the bluer-when-brighter trend using many epochs of broadband photometry. After correcting for the effects of broad emission lines (which are well known to be less variable than the continuum) in each filter, they compare their results to spectral variability predictions from accretion rate fluctuations in a simple thin disk, as well as more detailed static disk models. They find that accretion rate changes in these disk models *cannot* reproduce the strong bluer-when-brighter trend and instead suggest that ephemeral hot spots on the accretion disk may be needed (also see Trèvese & Vagnetti 2002; Meusinger & Weiss 2013).

The conclusions of Wilhite et al. (2005, hereafter WI05) and Schmidt et al. (2012, hereafter SC12) appear at first glance to be at odds: can the bluer-when-brighter trend observed in quasars be explained by fluctuations in the global accretion rate in a simple thin disk, or are localized temperature fluctuations needed? In this paper, we revisit the spectral variability study of WI05 using a larger sample of repeat quasar spectra culled from the full SDSS-I/II data set, to investigate these apparently discordant results. We will also compare our spectral variability results to the recently developed time-dependent model of inhomogeneous accretion disks by Dexter & Agol (2011). The structure of this paper is as follows: in Section 2, we describe the construction of the sample of repeat quasar spectra used in this study and our spectrophotometric recalibration. In Section 3, we discuss the properties of the quasars' difference spectra, as well as the construction of composite spectra and composite difference spectra. In Section 4, we compare our results to the previous studies of WI05 and SC12 using global accretion rate fluctuations in a thin disk. In Section 5, we discuss the quasar spectral variability predicted from a time-dependent model with temperature fluctuations and show that our observations are well fit by such inhomogeneous disks. In Section 6, we discuss the connection between disk properties and the resultant spectral variability, as well as other variability mechanisms that might match the observations. We summarize and conclude in Section 7.

2. DATA SELECTION AND REDUCTION

2.1. SDSS-I/II Repeat Spectra

All spectroscopic data used in our paper are from the SDSS-I/II, which is publicly available in its entirety as part of SDSS Data Release 7 (DR7; Abazajian et al. 2009). The SDSS-I/II obtained follow-up spectra of approximately 1.6×10^6 objects, including more than 1.1×10^5 quasars (Schneider et al. 2010), primarily selected by optical color from the imaging portion of the survey (Richards et al. 2002). The two fiber-fed SDSS spectrographs utilize a total of 640 fibers plugged into holes drilled onto plates, which are placed at the telescope focal plane. During the normal course of operations, multiple 15 minute exposures of each plate are taken, and spectra from exposures within approximately a month are typically coadded together. The spectral reduction and calibration using the SDSS Spectro2d pipeline are described in Stoughton et al. (2002). Occasionally, entire plates may be reobserved and coadded separately as a second epoch of spectra. This may occur if the first epoch did not reach sufficiently high signal-to-noise ratios (S/Ns), or in some cases by design as part of the survey plan. For these multiply observed plates, no attempt was made to ensure that the same fiber was plugged into the same hole on the plate, and so spectra of the same object may have different fiber numbers in the different epochs, even though the plate number is identical. For more details about these repeatedly observed plates, we refer to discussions in Wilhite et al. (2005).

Although multiple epochs of SDSS spectra are also possible due to spatial overlaps in the sky between adjacent plates, Vanden Berk et al. (2004) showed that additional calibrations based on non-variable stars on the same plates enhance sensitivity to the wavelength-dependent variability properties of quasars. Overlapping regions on adjacent plates are generally small and will not have many non-variable stars in the overlapping regions to accurately recalibrate the quasar spectra in the same regions. Thus, we focus only on multi-epoch spectra from plates that have been reobserved in their entirety, which ensures that multi-epoch spectra of many calibration stars are available in addition to the quasars. We also note that more epochs of spectra for many SDSS DR7 quasars are now publicly available as part of the SDSS-III Baryon Oscillation Spectroscopic Survey (Dawson et al. 2013). However, SDSS-III utilizes a newer spectrograph, fiber system, and spectral reduction pipeline; robust comparison of continuum properties of spectra between SDSS-I/II and SDSS-III is difficult and thus not considered here.

Using the plate list of 2880 observations of all 2698 unique plates in DR7 from SDSS-I/II, we select only those that are part of the main SDSS survey (and its primary reduction pipeline) by requiring the flag SURVEY = "sdss." A data quality cut is then made by requiring the flag PLATEQUALITY = "good" or "marginal"; plates that pass this quality cut have S/N > 9 and less than 13% problematic pixels. From the remaining plates, we select those that have multiple observations with time lag >30 days between each pair of epochs in the observed frame. This time-lag cut is physically motivated from photometric studies of quasar light curves, which have shown that quasars are generally not variable above ∼1% in flux on such short timescales (Kelly et al. 2009; Kozłowski et al. 2010; MacLeod et al. 2011). We note that a few plates had three or more observations; in such cases, we use all unique pairs of observations of each plate that pass all the above criteria. There are a total of 71 unique pairs of plate observations in SDSS-I/II,

Table 1
All Unique Pairs of Repeatedly Observed Plates in SDSS-I/II with Time Lag >30 days, PLATEQUALITY = "good" or "marginal," along with the Number of Quasars and Variable Quasars on Each Plate

Plate Number	High S/N MJD	Low S/N MJD	Quasars	Variable Quasars
291	51,660	51,928	21	9
293	51,994	51,689	54	18
296	51,578	51,984	26	7
297	51,663	51,959	23	15
300	51,666	51,943	41	6
301	51,641	51,942	45	17
304	51,957	51,609	26	12
306	51,690	51,637	35	1
309	51,666	51,994	47	14
340	51,691	51,990	24	3
351	51,780	51,695	36	3
352	51,789	51,694	29	6
360	51,780	51,816	69	6
385	51,783	51,877	49	5
390	51,816	51,900	30	7
394	51,876	51,812	31	6
394	51,812	51,913	28	5
394	51,876	51,913	31	5
404	51,877	51,812	14	1
406	51,817	51,869	48	6
406	51,876	51,817	50	4
406	51,817	51,900	49	5
406	52,238	51,817	48	19
406	51,900	51,869	54	6
406	52,238	51,869	47	19
406	52,238	51,876	51	19
406	52,238	51,900	49	20
410	51,816	51,877	83	22
411	51,873	51,817	28	8
412	51,871	51,931	30	3
412	51,871	52,235	29	8
412	51,871	52,250	31	8
412	51,871	52,254	30	13
412	51,871	52,258	29	11
412	52,235	51,931	32	12
412	52,250	51,931	35	13
412	52,254	51,931	32	11
412	51,931	52,258	32	11
413	51,821	51,929	46	3
414	51,869	51,901	39	3
415	51,879	51,810	39	4
416	51,885	51,811	68	31
418	51,884	51,817	72	16
419	51,812	51,868	69	7
419	51,812	51,879	64	24
422	51,878	51,811	26	1
476	52,027	52,314	80	20
483	51,942	51,902	78	8
525	52,029	52,295	52	19
547	51,959	52,207	66	19
662	52,178	52,147	37	5
803	52,264	52,318	4	1
810	52,326	52,672	4	0
814	52,370	52,443	47	7
820	52,405	52,438	80	3
960	52,466	52,425	31	1
1028	52,562	52,884	3	2
1034	52,525	52,813	2	1
1037	52,826	52,878	1	0
1512	53,035	53,742	19	7
1670	53,438	54,553	41	19
1782	53,383	53,299	31	3
1905	53,613	53,706	21	5
1907	53,265	53,315	27	3
2009	53,857	53,904	44	3
2061	53,405	53,711	17	8
2252	53,565	53,613	0	0
2294	54,524	53,733	63	37
2394	54,518	54,551	0	0
2474	54,333	54,564	7	1
2858	54,498	54,464	1	1

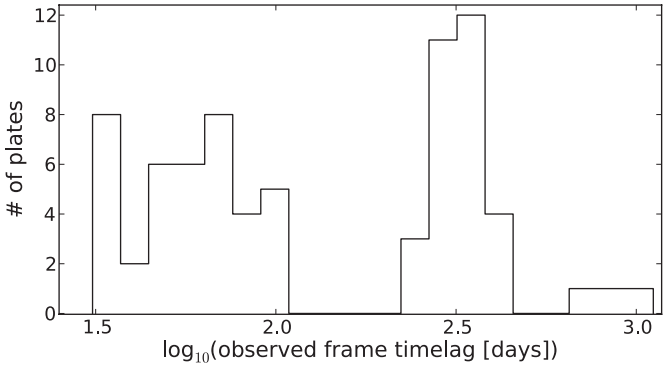

Figure 1. Distribution of the observed-frame time lags between repeat observations of the 71 pairs of plate observations used in our sample (listed in Table 1).

which are listed in Table 1. Figure 1 shows the distribution of the time lags for these 71 pairs of plate observations, which range from 30 days to about 3 yr in the observed frame.

2.2. Spectrophotometric Recalibration

We perform a wavelength-dependent spectrophotometric recalibration on all pairs of repeat quasar spectra on each plate, by first producing a "recalibration spectrum" for each pair of observations based on the non-variable stars on each plate. This is done following WI05 with only minor modifications, to allow for faithful comparison to previous work. We note here that to facilitate our difference spectra analysis, we have resampled all spectra and their uncertainties onto a common wavelength grid of the form $\log_{10}\lambda = 2.602 + 0.001a$, for integers a from 0 to 1400 (λ in Å units). This is approximately a factor of 10 coarser than the actual SDSS spectral resolution, but appropriate for our investigation of the continuum properties of quasars. The resampling is done using a simple linear interpolation, and the resulting common wavelength grid covers 400 to 10046 Å, wide enough for all rest-frame spectra of the quasars in our sample. As part of the interpolation to the common wavelength grid, we mask out problematic pixels in each spectrum that had SDSS pipeline flags set for NOPLUG, BADTRACE, BADFLAG, BADARC, MANYBADCOLUMNS, MANYREJECTED, NEARBADPIXEL, LOWFLAT, FULLREJECT, SCATTEREDLIGHT, NOSKY, BRIGHTSKY, COMBINEREJ, or REDMONSTER (for details on these flags, see Stoughton et al. 2002). We consider only pairs of repeat spectra of objects for which <20% of pixels are rejected in both epochs.

For each pair of plate observations, all pairs of stellar spectra are selected by requiring the SDSS Spectro1d pipeline classification of both spectra to have CLASS = "STAR" and their SUBCLASS classification to be identical between the two epochs. To remove the stars that have significantly varied

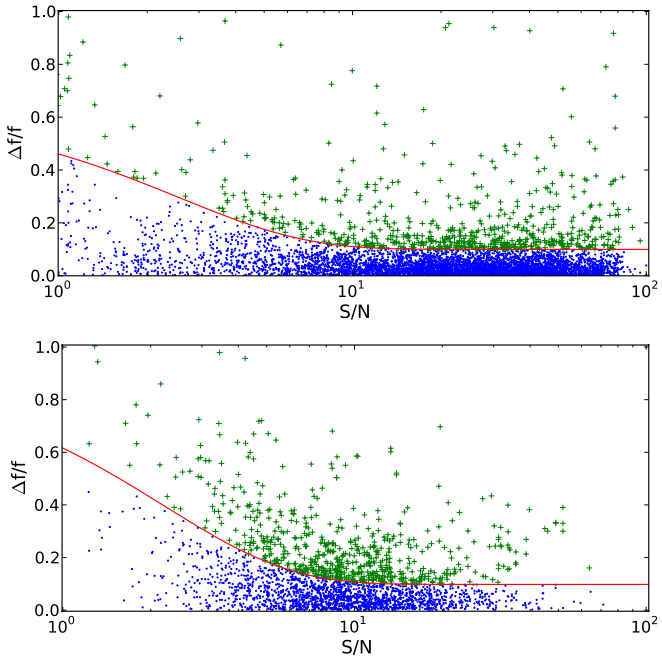

Figure 2. Top panel: relative flux change $\Delta f/f$ seen in repeat spectra of stars as a function of the S/N of the high-S/N epoch. The fitted exponential function (red solid line) divides stars deemed to be variable (green crosses) and non-variable (blue points). The non-variable stars are used to calculate a wavelength-dependent spectrophotometric recalibration for pairs of repeat spectra on each plate. Bottom panel: $\Delta f/f$ as a function of S/N, similar to the top panel, but for known quasars after applying our spectrophotometric recalibration. The sample of variable quasars defined here is used to produce the composite spectra in Figure 5.

(A color version of this figure is available in the online journal.)

between the two epochs, we integrate each pair of stellar spectra and calculate the relative change in flux of the star $\Delta f/f = |(f_1 - f_2)|/(0.5f_1 + 0.5f_2)$, where f_1 and f_2 are the integrated fluxes in the two epochs. Stars with large $\Delta f/f$ are unsuitable for use in the spectrophotometric recalibration due to their variability. Since $\Delta f/f$ is dependent on the S/N of the spectra, we follow the procedure of WI05 to include the flux uncertainties on the spectra in the variability selection by placing a variability cut on $\Delta f/f$ as a function of the S/N; Figure 2 shows the distribution of $\Delta f/f$ against the S/N of high-S/N epoch spectra for all stars on the 71 plates. We bin the stars in Figure 2 into 13 equally sized bins of S/N and calculate the 90th percentile in $\Delta f/f$ in each bin. We then fit an envelope with these 13 points of 90th percentile $\Delta f/f$ to an exponential function of the form $\Delta f/f = 0.53\exp(\mathrm{S/N}-0.57) + 0.10$. Stars with $\Delta f/f$ below this envelope are considered "non-variable" (Figure 2) and are used in the subsequent spectrophotometric recalibration. There were 6327 stars in total over the 71 plates, 5615 of which were deemed to be non-variable. On a typical plate, a median of 47 non-variable stars were used in the spectrophotometric recalibration.

For each pair of non-variable stellar repeat spectra, we take the ratio of the lower-S/N epoch spectrum to the higher-S/N epoch spectrum; for a non-variable star for which the two epochs of spectra are perfectly calibrated, this results in a flat ratio spectrum with ratio 1. However, plate-wide wavelength-dependent systematic calibration differences between the two epochs may be present. We take the median ratio spectrum of all non-variable stars on each plate and interpolate a fifth-order polynomial to reduce the effects of noise. Prior to the interpolation, we clip the top and bottom 3rd percentile of pixels in the ratio spectrum to avoid skewing the interpolation from outlying pixels. The low-S/N epoch spectra of all quasars on each plate will be multiplied by this interpolated median ratio spectrum to match the calibration of the high-S/N epoch spectra. The interpolated median ratio spectra used in the spectrophotometric recalibration are generally a <5% correction at all wavelengths and are almost all <10%, consistent with the findings of WI05.

To select all quasars in these 71 pairs of repeat plate observations, we match all spectra to the SDSS DR7 quasar catalog (Schneider et al. 2010) to find a total of 2626 quasars, and we apply the wavelength-dependent spectrophotometric recalibration for all quasars on each plate. Comparison of repeat spectra for objects that did not significantly vary between the two epochs will be dominated by noise, and so we place an S/N-dependent variability cut on the $\Delta f/f$ for each quasar, similar to the stars, but now to select variable quasars. After binning the quasars into 13 equal bins of S/N, we fit an exponential to the 75th percentile $\Delta f/f$ in each bin of the form $\Delta f/f = 0.81\exp(\mathrm{S/N}-0.22)+0.10$. We have used the 75th percentile $\Delta f/f$ in the variability cut rather than the 90th percentile used in the stellar case because quasars are known to be more strongly variable than stars in general (Sesar et al. 2007). Out of 2626 quasars on the 71 plates, 626 are selected as spectroscopic variables. We note that by design, this sample of quasars we use to study spectral variability are those exhibiting the strongest variability; this is desirable for the present study to ensure high S/N of the spectral variability results.

3. QUASAR DIFFERENCE SPECTRA

3.1. Difference Spectra and Their Properties

Before construction of difference spectra using the 626 pairs of variable quasar spectra selected in Section 2, we shift each spectrum to the rest frame using visually inspected redshifts from Schneider et al. (2010). To ensure that the resulting difference spectra are "positive," we subtract the spectral epoch with the lower integrated flux from the higher, with uncertainties added in quadrature. The continuum of each difference spectrum should thus be bluer than either of the individual epochs if these quasars exhibit a bluer-when-brighter trend. We visually inspect all 626 pairs of spectra along with their difference spectra and find that the continuums of the difference spectra are well fit by power laws and indeed show the bluer-when-brighter trend in the vast majority of cases. In the visual inspection, we identify 11 pairs of spectra that show evidence for strong broad absorption lines (BALs). BAL quasars are known to have atypical continuum properties (e.g., Reichard et al. 2003; Gibson et al. 2009), and the BALs are known to exhibit intrinsic variability in their absorption-line strengths over long timescales (e.g., Gibson et al. 2008, 2010; Capellupo et al. 2011, 2012; Filiz Ak et al. 2012, 2013). To avoid contamination, we remove these 11 BAL quasars from our sample. We also remove 11 additional quasars identified in the visual inspection for which the variability was clearly dominated by noise. The remaining sample of 604 quasars is the sample for which all further results from our analysis are reported.

We fit the continuum of each difference spectrum to a power law using a simple χ^2 fit, incorporating the uncertainties in the difference spectra. Although broad emission lines are well known to be less variable than the continuum (WI05), there is still evidence of emission-line variability in our difference spectra. Thus, we mask out the following wavelength

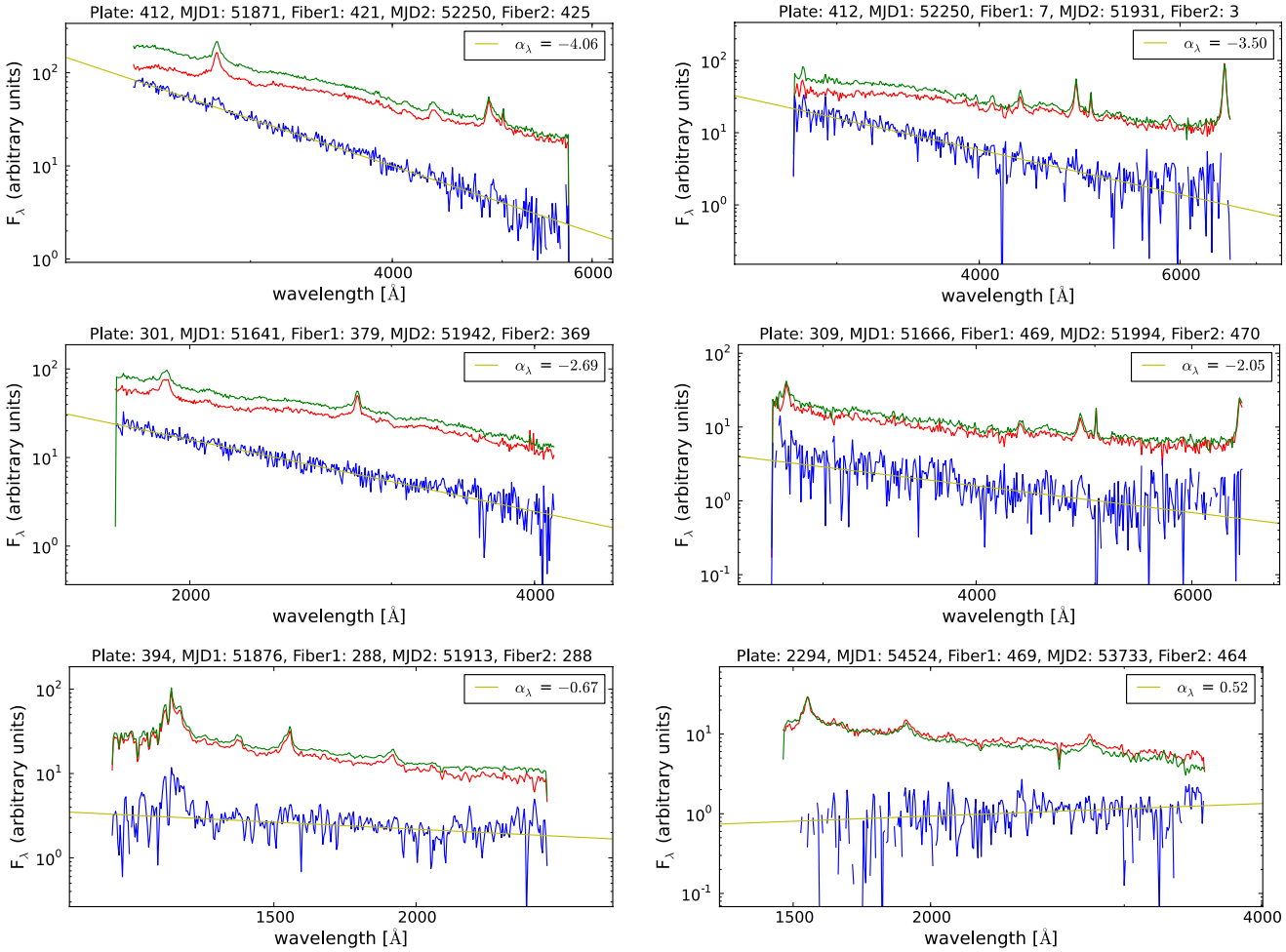

Figure 3. Examples of pairs of repeat variable quasar spectra (green and red), their difference spectra (blue), and best-fit power laws to the difference spectra continuum (yellow), for a range of power-law indices of the difference spectrum. All spectra shown are corrected for Galactic extinction and are scaled to arbitrary flux densities. The vast majority of the repeat quasar spectra in our sample show a strong bluer-when-brighter trend.

(A color version of this figure is available in the online journal.)

regimes dominated by broad emission lines in the continuum fitting: 1360–1446 Å (Si IV, O IV]), 1494–1620 Å (C IV), 1830–1976 Å (C III], Fe III), 2686–2913 Å (Mg II), 4285–4412 Å (Hγ), 4435–4762 Å (Fe II), 4760–4980 Å (Hβ), 4945–4972 Å ([O III]), 4982–5035 Å ([O III]), and 5100–5477 Å (Fe II), as well as wavelengths <1300 Å to avoid Lyα emission and absorption. The choice of these masked regions is informed by the composite SDSS quasar spectrum of Vanden Berk et al. (2004); the numerous other lines and line complexes present in quasar optical spectra that we do not mask out tend to be less prominent, and we do not find evidence that these other emission lines significantly affect the continuum fitting in our visual inspections. We clip the top and bottom 1st percentile of pixels in each spectrum after applying these masks (but before the fitting) to avoid strong outliers. After the first power-law fit, we again clip the top and bottom 1st percentile of pixels away from the best-fit power law, before refitting the final time.

Figure 3 shows a few examples of pairs of quasar spectra and their difference spectra from our sample, for a range in fitted power-law spectral indices α_λ (where $F_\lambda \propto \lambda^{\alpha_\lambda}$) of the difference spectra continua. The difference spectra show excellent fits to a simple power law and a strong bluer-when-brighter trend. Figure 4 shows the distribution of the spectral indices of the difference spectra for all 604 quasars, with and

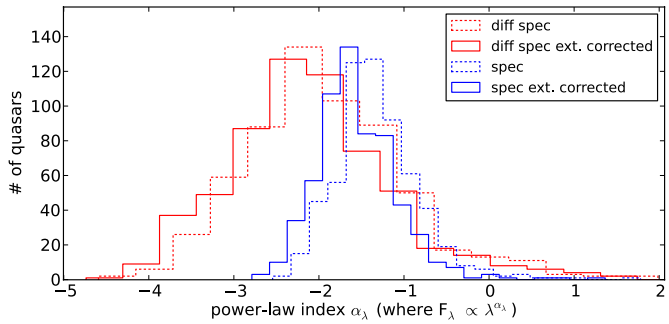

Figure 4. Distribution of fitted power-law spectral indices α_λ for the high-S/N epoch spectra of all variable quasars in our sample (blue dotted lines), and for their difference spectra (red dotted lines) without correcting for Galactic extinction. The distributions of the fitted indices for the same quasars after correcting for Galactic extinction are shown in solid lines. The median of these distributions is an excellent match to previous studies.

(A color version of this figure is available in the online journal.)

without corrections for Galactic extinction using the extinction maps of Schlegel et al. (1998) and the reddening law of Cardelli et al. (1989). To compare the difference spectra to the underlying spectra, we also calculate power-law spectral indices of the continua from the high-S/N epoch in each pair of repeat-quasar

spectra; this provides a relatively unbiased view of the general spectral properties of each quasar. The fitting of the continua of the spectra to a power law is performed similarly to the difference spectra, but with an additional wavelength region mask of all wavelengths >5800 Å to avoid contamination from host-galaxy emission (Vanden Berk et al. 2004). As expected, Figure 4 shows that quasar difference spectra are generally bluer than single-epoch quasar spectra, and the addition of corrections for Galactic extinction causes the continuum spectral indices to become even bluer.

3.2. Composite Spectrum and Difference Spectrum

We construct a geometric mean composite spectrum for both the difference spectra and the high-S/N single-epoch spectra of the 602 quasars in our sample with corrections for Galactic extinction; the use of a geometric mean to construct the composite spectrum preserves the arithmetic mean power-law spectral indices and extinction of a sample of power-law spectra (Reichard et al. 2003), well suited for our investigation of quasar continuum properties. The composite spectra are created by using our power-law fits to the high-S/N epoch and difference spectra for each pair of spectra, and scaling the flux density of the fitted power laws at 3062 Å (a relatively line-free wavelength and covered by nearly all of the spectra in our sample) to a fixed arbitrary flux density. The spectra and difference spectra themselves are then each rescaled by the same scaling factor as their fitted power laws, and a geometric mean of all rescaled spectra and difference spectra in each wavelength bin is taken to produce the composites. The geometric mean composite spectrum and composite difference spectrum are shown in Figure 5. The 1σ uncertainties on the composite spectrum and difference spectrum are estimated by resampling all the pixel flux densities in each spectrum from a Gaussian with center at the measured flux density and width set to the uncertainty in the flux density. All 604 pairs of spectra are resampled 10^3 times, and 10^3 composite spectra and composite difference spectra are produced. The 1σ uncertainties shown are the 1σ spreads in these 10^3 resampled composites around the mean.

We fit the continuum of the composite spectrum and composite difference spectrum using the same broad emission line wavelength masks as before to find a power-law spectral index of $\alpha_{\lambda,\mathrm{comp}} = -1.56 \pm 0.01$ for the composite spectrum and $\alpha_{\lambda,\mathrm{diff}} = -2.12 \pm 0.02$ for the composite difference spectrum. Without corrections to each spectrum for Galactic extinction (not shown), the spectral indices are $\alpha_{\lambda,\mathrm{comp}} = -1.38 \pm 0.01$ and $\alpha_{\lambda,\mathrm{diff}} = -1.94 \pm 0.02$. We note that although the host-galaxy emission that dominates the composite quasar spectrum redward of ~6000 Å should not be time variable, the composite difference spectrum seems to show some host-galaxy emission residuals. This is predominately due to noisy data and poorly subtracted masked pixels at the red edge of the spectra, as well as the fact that the number of spectra contributing to the composite at wavelengths >6000 Å is only ~50 out of a total sample of 604. The composite difference spectrum is thus unreliable at >6000 Å.

4. COMPARISON TO PREVIOUS STUDIES

Our analysis thus far has closely followed the work of WI05, and in this section we compare our results to those from previous studies. For the composite quasar spectrum continuum, our calculated spectral index $\alpha_{\lambda,\mathrm{comp}} = -1.56 \pm 0.01$ with corrections for Galactic extinction is an exact match to the results

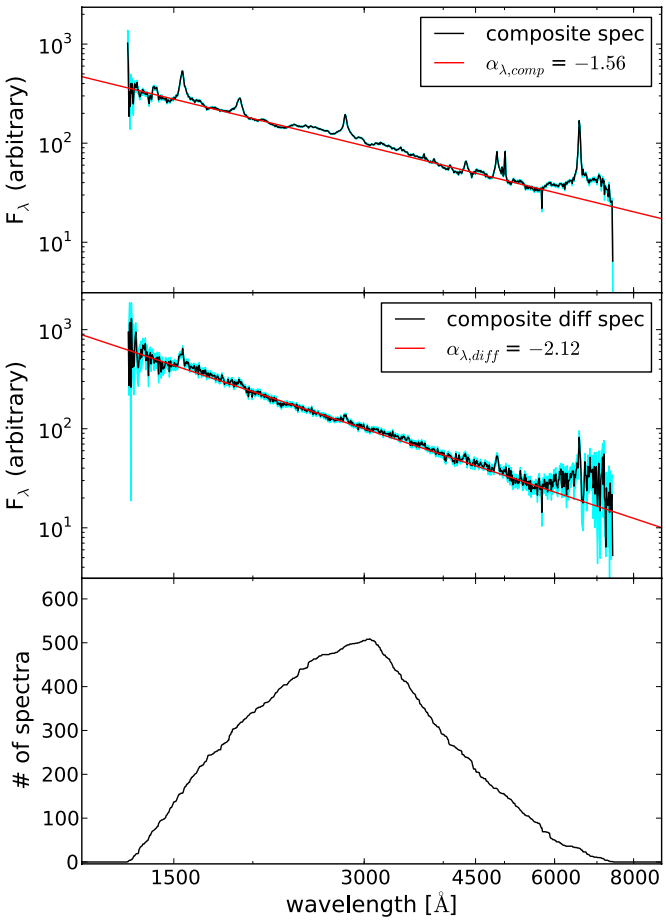

Figure 5. Top panel: geometric mean composite quasar spectrum of all high-S/N epoch spectra in our sample of 602 variable quasars, corrected for Galactic extinction, with 1σ uncertainties shown in light blue. The fitted power-law index of the continuum ($\alpha_{\lambda,\mathrm{comp}} = -1.56$) is in excellent agreement with the composite SDSS quasar spectrum of Vanden Berk et al. (2004) for $\lambda < 5000$ Å, where host-galaxy light is minimal. Middle panel: geometric mean composite quasar difference spectrum for the pairs of variable quasars in our sample, corrected for Galactic extinction, with 1σ uncertainties shown in light blue. The fitted power-law index of the continuum ($\alpha_{\lambda,\mathrm{diff}} = -2.12$) is steeper than that of the composite spectrum, showing that the majority of quasars exhibit a bluer-when-brighter trend. Bottom panel: number of spectra contributing to the composite spectrum and composite difference spectrum at each wavelength.
(A color version of this figure is available in the online journal.)

of Vanden Berk et al. (2004), while our $\alpha_{\lambda,\mathrm{comp}} = -1.38 \pm 0.01$ without corrections for Galactic extinction is an excellent match to the $\alpha_{\lambda,\mathrm{comp}} = -1.35$ calculated by WI05, all based on SDSS-I/II spectra in a similar range of wavelengths. For the composite quasar difference spectrum continuum, our calculated $\alpha_{\lambda,\mathrm{diff}} = -1.94 \pm 0.02$ without corrections for Galactic extinction is also an excellent match to the $\alpha_{\lambda,\mathrm{diff}} = -2.00$ from WI05. The minor discrepancy is likely due to differences in sample size, as our sample of 602 quasars is approximately a factor of two larger than the sample used in WI05 (although of course many objects are in common).

Pereyra et al. (2006) utilized the composite difference spectrum generated by WI05 and showed that it is well fit by synthetic difference spectra generated from a thin-disk model that has undergone some change in its global accretion rate. However, difference spectra are subject to both Galactic and intrinsic (host-galaxy) extinction; the composite difference spectrum of WI05 was not corrected for any extinction and thus should not be directly compared to models. Although we have corrected

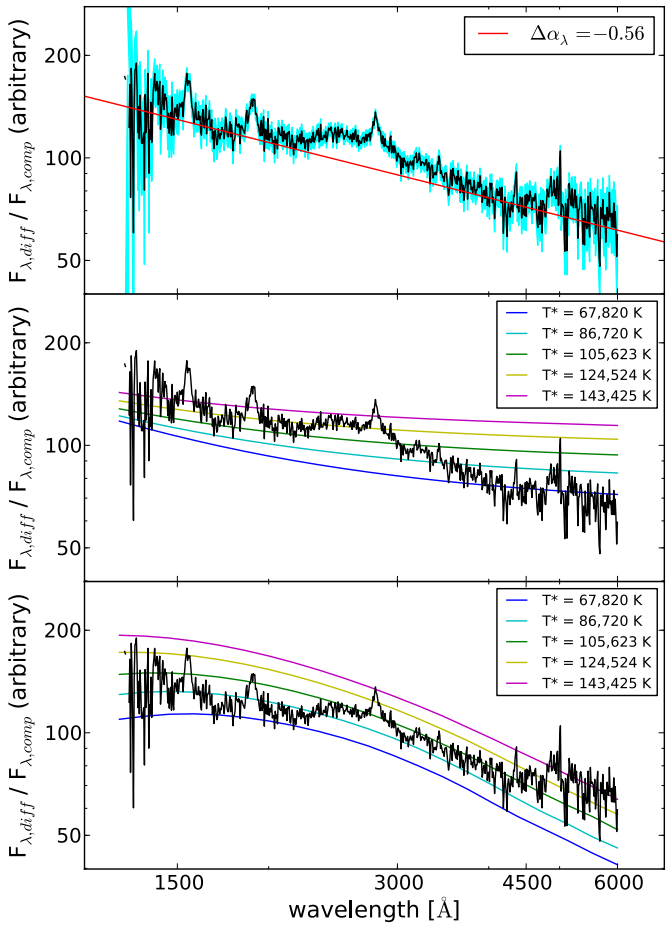

Figure 6. Top panel: observed composite relative variability spectrum, created by dividing the composite difference spectrum by the composite spectrum from Figure 5, with 1σ uncertainties shown in light blue. The best-fit power law to the continuum is shown (red), with relative spectral index $\Delta\alpha_\lambda \equiv \alpha_{\lambda,\mathrm{diff}} - \alpha_{\lambda,\mathrm{comp}} = -0.56$. We note that we have flipped this spectrum in the vertical direction around the best-fit power-law continuum (see the text for details). Middle panel: comparison of the relative variability spectrum to that generated from changing the accretion rate in a thin-disk model by 5%. The resulting synthetic relative variability spectra for a range of thin-disk characteristic temperatures are shown; none are as steep as the observations, and thus they do not display as strong of a bluer-when-brighter trend. Bottom panel: same as the middle panel, but instead comparing synthetic relative variability spectra generated from an inhomogeneous accretion disk with large temperature fluctuations. This model provides a good match to our observations in the optical.

(A color version of this figure is available in the online journal.)

each spectrum for Galactic extinction in our work, the intrinsic extinction of each quasar is much more difficult to take into account. Thus, our composite difference spectrum is subject to unknown amounts of intrinsic extinction from each of the individual quasars in the sample.

To avoid issues with extinction and robustly compare our observed spectral variability to models, we instead consider the spectral variability *relative* to the underlying spectra of the quasars, by dividing the geometric mean composite difference spectrum by the geometric mean composite spectrum from Figure 5. The result, which we call the "relative variability spectrum," is shown in Figure 6 and has a power-law spectral index of $\Delta\alpha_\lambda \equiv \alpha_{\lambda,\,\mathrm{diff}} - \alpha_{\lambda,\,\mathrm{comp}} = -0.56 \pm 0.02$. The result of this division of geometric mean composite spectra is independent of any extinction with the reasonable assumption that the extinction does not significantly change between each pair of observations. We note that because broad emission lines are less variable than the continuum, the relative variability spectrum will have inverted emission lines; we have flipped the relative variability spectrum in Figure 6 in the vertical direction, centered on the best-fit continuum to aid in identifying continuum and emission features visually. The spectral variability of quasars relative to their underlying spectra was also investigated in WI05 using the ratio between composite difference spectra and composite spectra of their quasar sample, leading WI05 to conclude that quasars exhibited spectral variability only at wavelengths <2500 Å. However, this was done by WI05 using arithmetic mean composites, which do not preserve the mean power-law indices of the spectra (making interpretation difficult), and is subject to the effects of extinction. In contrast to WI05, our relative variability spectrum avoids both these issues by using geometric mean composite spectra, facilitating robust comparison to models.

In Figure 6 (middle panel), we compare our observed relative variability spectrum to synthetic relative variability spectra generated from thin-disk models in which the global accretion rate has increased by 5%, for a range in characteristic disk temperatures

$$T^* \equiv \left\{ \frac{3\dot{M}GM_{\mathrm{BH}}}{8\pi r_i^3 \sigma_s} \right\}^{1/4} \quad (1)$$

(Frank et al. 2002). The range in T^* in Figure 6 (middle panel) is chosen to span the full range generated for thin disks with $\log_{10}L/L_{\mathrm{Edd}} = [-1.1, -0.8]$ and $\log_{10}M_{\mathrm{BH}} = [8.5, 9.5]$. These ranges in $\log_{10}L/L_{\mathrm{Edd}}$ and $\log_{10}M_{\mathrm{BH}}$ are representative of these values in our sample of 604 quasars, which have median $\log_{10}L/L_{\mathrm{Edd}} = -0.89$ and median $\log_{10}M_{\mathrm{BH}} = 8.83\ M_\odot$ from the catalog of Shen et al. (2011). From the spectral variability shown in Figure 6 (middle panel), it is clear that a scenario in which a thin disk changes its global accretion rate cannot account for the strong bluer-when-brighter trend observed in quasars, and it does not produce our observed power-law relative variability spectrum. Our spectral variability evidence against global accretion rate fluctuations as the cause of quasar flux variability is independently in agreement with the argument that quasar accretion disks are too large to vary coherently. We note that although we have shown in Figure 6 (middle panel) difference spectra of a thin disk in which the accretion rate changed by 5%, the shapes of difference spectra from thin-disk models with accretion rate fluctuations are not particularly sensitive to the exact change in accretion rate (i.e., the fit will not significantly improve by increasing the change in accretion rate). Instead, the difference spectra from thin-disk models depend mainly on the disk's characteristic temperature, for which we have shown a wide range in Figure 6 (middle panel). A similar conclusion was reached by Pereyra et al. (2006).

Aside from our results, the photometric quasar spectral variability study of SC12 also argued against global accretion rate changes as the sole driver in quasar spectral variability. We suggest that the source of the discrepancy between the conclusions of SC12 and Pereyra et al. (2006) may be due to their subtly different parameterizations of quasar spectral variability and its effects on the extinction. SC12 fitted linear relations to multi-epoch photometry of quasars in several filters in magnitude–magnitude space and transformed the relation into color–magnitude space to investigate the variability in different filters. The spectral variability parameter that SC12 compared to models was the slope of the fit in color–magnitude space after the transformation; this slope was fit after all magnitudes for each quasar were normalized to its mean magnitudes for the different

filters (see Equation (3) in SC12) and thus parameterizes the spectral variability of each quasar *relative* to its underlying color. This parameterization is similar to the power-law spectral index of the relative variability spectrum ($\Delta\alpha_\lambda$) we calculate, but for photometric colors, and is thus also independent of extinction. Although this subtlety was not discussed in SC12, this may be the source of the conflicting results between SC12 and Pereyra et al. (2006) in comparing their observations to global accretion rate fluctuations in a thin disk.

Aside from a simple thin disk, SC12 also compared their spectral variability results to more sophisticated models presented in Davis et al. (2007), finding that their data cannot be explained by accretion rate changes in any of these disk models. SC12 suggested that ephemeral hotspots may be needed to match their observations; in the next section, we compare our observed results to one such time-dependent model of a simple inhomogeneous disk.

5. DISK MODELS WITH LOCALIZED TEMPERATURE FLUCTUATIONS

Dexter & Agol (2011) presented a simple analytic model of a time-dependent inhomogeneous disk, based on a thin disk radiating with independent zones undergoing temperature fluctuations and emitting locally as a blackbody. Aside from predictions of MHD turbulence in simulations of accretion disks, there is now also observational evidence for disks with time-dependent temperature fluctuations from microlensing disk-size measurements, the strong UV spectral continuum, and single-band variability characteristics. Dexter & Agol (2011) find that to satisfy these observational constraints, accretion disks must be *strongly* inhomogeneous, with large localized temperature fluctuations. These large temperature fluctuations in the disk inhomogeneities will likely cause the spectrum to be highly variable at short wavelengths and produce distinct spectral variability with which we will compare our observations.

We set up the inhomogeneous accretion disk model of Dexter & Agol (2011), starting with a standard thin disk with an inner edge at the innermost stable circular orbit of a non-spinning black hole, and dividing its surface into n zones per factor of two in radius. The zones are roughly equally divided radially and azimuthally, although the exact setup does not noticeably affect the results in our tests. The logarithmic temperature $\log_{10}T$ in each zone independently fluctuates as a first-order continuous autoregressive (CAR(1)) process, motivated by studies of single-band variability characteristics (e.g., Kelly et al. 2009). The mean temperature in each zone is set to the $\log_{10}T$ of the thin-disk model at that radius, and the constant driving the $\log_{10}T$ fluctuations in the CAR(1) process is σ_T. The characteristic decay timescale of the temperature fluctuations is set to 200 days in the rest frame, motivated by the observed timescales in Kelly et al. (2009) and MacLeod et al. (2010). Our spectral variability results are not sensitive to the choice of this timescale, although we note that if the decay timescale is significantly longer than the time lag between repeat observations, the quasar will not appear to be significantly variable. All regions in the inhomogeneous disk are assumed to emit locally as a blackbody, and no relativistic effects are considered in this simple model.

We run the inhomogeneous disk model, sampling its spectrum in the wavelength range of 1300–5800 Å at 50 day intervals in the rest frame, after an initial "burn-in" time of 500 days to allow the disk to become inhomogeneous. To faithfully compare to our observations, we calculate the change in observable flux between successive time steps by integrating the spectrum, and we calculate the difference spectrum between any two successive time steps in which the total flux changed by more than 10%, similar to the variability cut placed on the observed spectra in Figure 2. We run the model until we produce 5×10^3 synthetic difference spectra, and we produce a synthetic geometric mean composite spectrum and composite difference spectrum, by renormalizing each spectrum in the same way as our SDSS spectra.

Figure 7 shows synthetic relative difference spectra generated from the inhomogeneous disk model over a range in independent zones n and temperature fluctuations σ_T, for the same disk temperatures as shown in Figure 6. The inhomogeneous disk produces relative variability spectra with a characteristic shape that is a power law at optical wavelengths, which flattens at shorter wavelengths in the UV. For increasing n and σ_T in Figure 7, the relative variability spectra remain power-law-like further into the UV before flattening (the physical cause of this is discussed in Section 6.1). Thus, to produce the observed power-law spectral variability in Figure 6 (top panel), the inhomogeneous disk needs to have many independent zones (large n) with large temperature fluctuations (large σ_T).

An example comparison of our observed relative variability spectrum to that from the inhomogeneous disk, using parameters $n = 10^{2.7}$ and $\sigma_T = 0.45$, is shown in Figure 6 (bottom panel). The large temperature fluctuations and number of fluctuating zones required of inhomogeneous disks to provide such good fits to our observations are in excellent agreement with the $n = 10^{2.5-3}$ and $\sigma_T = 0.35$–0.5 range found by Dexter & Agol (2011) to simultaneously satisfy independent observational constraints from microlensing disk-size measurements, their strong UV spectral continuum, and single-band variability characteristics of quasars. This independent result based on spectral variability adds to the mounting evidence for large temperature fluctuations in strongly inhomogeneous quasar accretion disks. We note that because the relative variability spectrum is constructed from composite spectra and composite difference spectra of many quasars, each with different Eddington ratios and disk temperatures, the fit of the inhomogeneous disk relative variability spectrum is likely to improve with a more complete consideration of these variations.

6. DISCUSSION

6.1. The Connection between Disk Properties and Resultant Spectral Variability

Our success in modeling quasar spectral variability in the previous section can be understood as the result of the confluence of large temperature fluctuations in a strongly inhomogeneous disk emitting locally as a blackbody. A flare in a portion of the disk causes the variable part of its optical spectrum to be due to the blackbody emission from the flaring region. For very high temperature flares, the blackbody spectrum of the flaring region peaks well into the UV, and thus the difference spectrum is dominated by its power-law Rayleigh–Jeans tail. This is the cause of the trend in Figure 7 where the power-law portion of the model relative variability spectrum increasingly extends into the UV as σ_T increases. We note that for small σ_T, the turnover in the UV is a flattening rather than a sharp peak because it is the superposition of the blackbody peaks of numerous flaring regions.

Aside from the large temperature fluctuations, the disk must also be strongly inhomogeneous, with a large number of

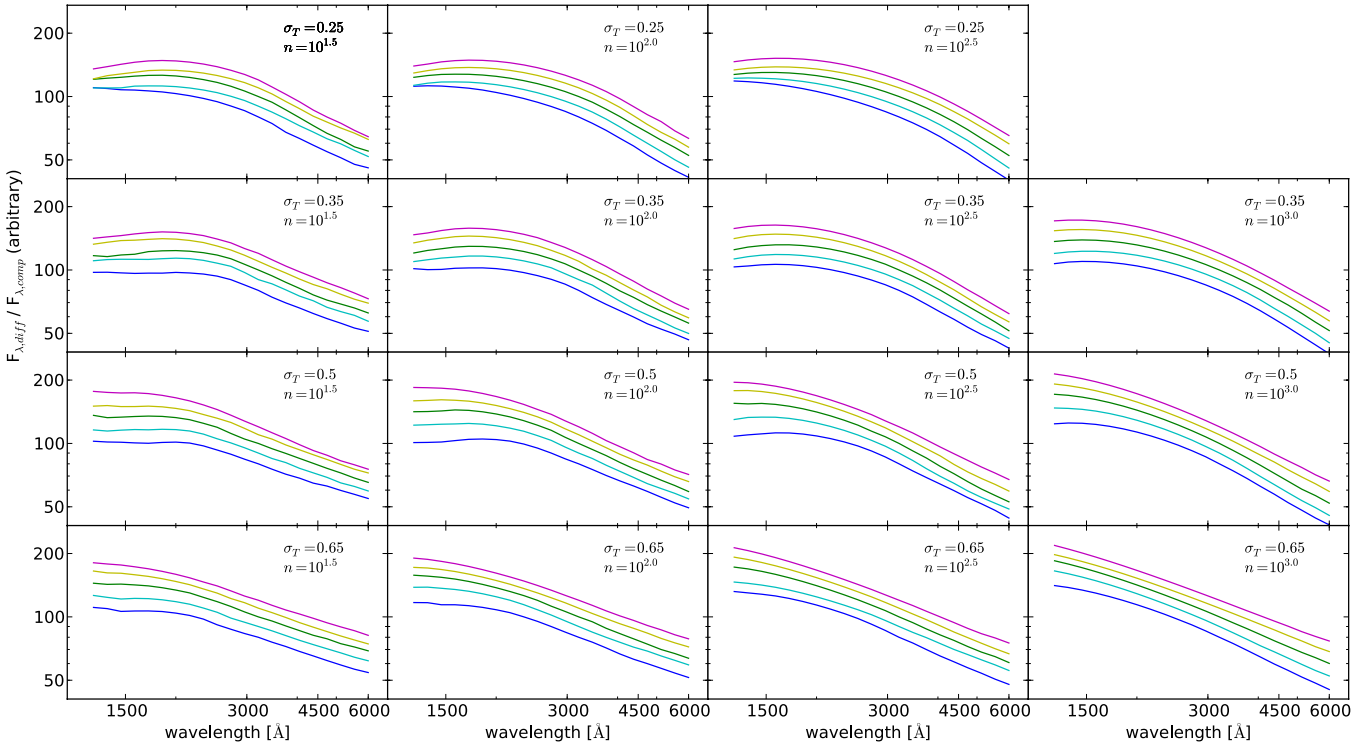

Figure 7. Synthetic relative variability spectra generated from the inhomogeneous disk over disk parameters σ_T and n (see Section 5 for details). The range in disk temperatures shown for each panel is the same as in Figure 6 (middle panel). These synthetic relative variability spectra are power laws in the optical, with a flattening in the UV. The turnover occurs further into the UV with both increasing σ_T and n (see Section 6.1 for discussion). Note that we do not show results for larger n and smaller σ_T because disks with these parameters are not variable enough in flux to produce difference spectra that pass our 10% flux change cut.

(A color version of this figure is available in the online journal.)

independently fluctuating regions (i.e., a disk with large n). This is due to the fact that the total flux variability amplitude of the disk scales as N^{-1}, where N is the number of independently varying zones (Dexter & Agol 2011); as n increases and the disk becomes more strongly inhomogeneous, the total flux variability decreases. In the case of a disk with small n, the difference spectra will be dominated by smaller, lower-temperature flares with blackbody peaks in the optical rather than the UV, and thus the spectral variability will not be dominated by the Rayleigh–Jeans spectrum. Conversely, for large n, the disk does not exhibit strong overall flux variability, and only very large, high-temperature flares are actually observable. Thus, the observed flux variability in strongly inhomogeneous disks will be dominated by the Rayleigh–Jeans spectrum, naturally producing power-law spectral variability. This effect causes the power-law portion of the model relative variability spectrum in Figure 7 to extend further into the UV with increasing n. We emphasize that this line of evidence for large temperature fluctuations in strongly inhomogeneous disks is independently in excellent agreement with other observational constraints from microlensing disk sizes, their strong UV spectral continuum, and single-band variability properties.

We note that because the temperatures in each independently fluctuating zone are damped in the CAR(1) process and thus cannot increase infinitely, the inhomogeneous disk predicts a flattening in the relative variability spectrum in the UV (e.g., as seen in Figure 7). This flattening is not seen in our difference spectra, which appear to be well fit by a power law down to ∼1300 Å, although the S/N decreases dramatically below ∼1500 Å. Broadband studies of quasar UV variability have shown that quasars are indeed generally more variable in the UV than optical (Gezari et al. 2013). However, a more careful investigation of quasar spectral variability from optical to the UV will require contemporaneous optical–UV observations and will be a fruitful test of the inhomogeneous disk model. We also note that in the simple inhomogeneous disk model of Dexter & Agol (2011), the global accretion rate is assumed to be constant. This may not be entirely justified, as processes causing the large temperature fluctuations such as the MRI are likely to also induce fluctuations in the accretion rate (e.g., by causing the viscosity to change locally). Although we have ruled out accretion rate fluctuations as the sole driver of quasar spectral variability in Section 4, the observed difference spectra in Figure 5 (middle panel) may still be affected by changes in the accretion rate. In particular, because Figure 6 (middle panel) shows that accretion rate changes produce spectral variability that is particularly strong in the UV, the addition of accretion rate changes to the inhomogeneous disk model may cause difference spectra to become power-law-like well into the far-UV, further improving the match to the observed UV spectral variability.

6.2. Other Possibilities for Difference Spectra

The disk models we have considered all assume that the disk emits locally as a blackbody; while this may be a good approximation for the underlying disk spectrum, it is not entirely justified for difference spectra, which instead isolate the variable part of the spectrum. It is possible that the observed power-law difference spectrum is instead at least partially due to non-thermal emission, which could dominate the variable portion of quasar optical/UV spectra. For example, disk inhomogeneities from the photon bubble instability in the magnetized atmosphere of a radiation-pressure-dominated disk (Arons 1992; Gammie 1998; Turner et al. 2005) may cause the spectrum during flaring epochs to become non-thermal, due to the shorter paths

in the low-gas-density bubbles for photons to diffuse to the photosphere (Gammie 1998), or due to an increase in free–free emission in the high-photon-density bubbles (Davis et al. 2009). Radio-loud quasars have long been suspected to harbor weak or unresolved jets, and the highly variable jet synchrotron emission can also produce power-law difference spectra in the optical/UV. Future observations of quasar spectral variability across multiple wavelength regimes contemporaneously can help constrain these possibilities.

6.3. Variability Correlations with M_{BH} and Luminosity

Finally, we note that our findings that quasar spectral variability cannot be driven purely by global accretion rate changes in a thin disk are not at odds with the trends between variability amplitude, black hole mass, and luminosity that many studies have found, and which suggest that the Eddington ratio may be driving these trends. It is still possible that differences in the mean Eddington ratio among different quasars drive their variability properties, a conclusion also reached by SC12. Notably, MacLeod et al. (2010) also found that the scaling relation between these quantities is much shallower than that predicted from the Eddington ratio, suggesting that additional physics may be necessary to explain the observed trend. Modeling of these trends using inhomogeneous disk models awaits future investigation.

7. CONCLUSIONS

The characteristic flux variability of quasars reflects complex processes in the accretion disk, yet the cause of the variability is still unknown. Aside from single-band variability characteristics, the spectral variability of quasars provides an additional, independent constraint on models of the variability mechanism. Using repeat spectra of quasars in SDSS-I/II, we investigate the optical spectral variability of quasars, which are known to show a bluer-when-brighter trend. After a wavelength-dependent spectrophotometric recalibration of the quasar spectra using non-variable stars observed on the same plates, we construct difference spectra of 602 variable quasars in our sample, thus isolating the variable part of the spectrum. We compare our observations to synthetic difference spectra generated from a thin-disk model in which the accretion rate has varied, as well as a simple inhomogeneous disk model with localized temperature fluctuations. In particular, we find the following.

1. Quasar difference spectra appear to be power laws with spectral indices steeper than their single-epoch spectra, indicating that the vast majority of quasars show a bluer-when-brighter trend. We measure quasar spectral variability using the relative variability spectrum, which is independent of any extinction. We find that accretion rate fluctuations in a thin-disk model cannot produce the strong bluer-when-brighter trend observed. This is contrary to the results of some previous investigations and may be due to the effects of intrinsic and Galactic extinction that were not accounted for in those previous studies.
2. A time-dependent inhomogeneous disk model can produce spectral variability that provides a good match to our observations over optical wavelengths if the disk is strongly inhomogeneous, with large temperature fluctuations. The difference spectra produced by such inhomogeneous disks are dominated by the Rayleigh–Jeans spectrum from the hot "flaring" regions in the optical and are thus naturally power laws. The large temperature fluctuations and large number of zones in the disk required to match our observed spectral variability are in excellent agreement with independent observational constraints from quasar microlensing disk sizes, their strong UV spectral continuum, and single-band flux variability characteristics.

Our spectral variability constraints suggest that future quasar disk models should be time dependent and include large temperature fluctuations. Improved global GRMHD simulations of radiative disks will help inform more sophisticated inhomogeneous disk models to compare to observations. Observationally, future time-domain photometric and spectroscopic observations from the Large Synoptic Survey Telescope (Ivezic et al. 2008) and the Time-Domain Spectroscopic Survey portion of SDSS-IV will help better constrain these models.

J.J.R. thanks Yusra AlSayyad and James R. A. Davenport for helpful discussions about processing SDSS spectra. Support for J.J.R. was provided by NASA through Chandra Award Numbers AR9-0015X, AR0-11014X, and AR2-13007X, issued by the Chandra X-ray Observatory Center, which is operated by the Smithsonian Astrophysical Observatory for and on behalf of NASA under contract NAS8-03060. Support for E.A. was provided by NASA through a grant from the Space Telescope Science Institute, which is operated by the Association of Universities for Research in Astronomy, Inc., under NASA contract NAS 5-26555.

Funding for the SDSS and SDSS-II has been provided by the Alfred P. Sloan Foundation, the Participating Institutions, the National Science Foundation, the U.S. Department of Energy, the National Aeronautics and Space Administration, the Japanese Monbukagakusho, the Max Planck Society, and the Higher Education Funding Council for England. The SDSS Web site is http://www.sdss.org/.

The SDSS is managed by the Astrophysical Research Consortium for the Participating Institutions. The Participating Institutions are the American Museum of Natural History, Astrophysical Institute Potsdam, University of Basel, University of Cambridge, Case Western Reserve University, University of Chicago, Drexel University, Fermilab, the Institute for Advanced Study, the Japan Participation Group, Johns Hopkins University, the Joint Institute for Nuclear Astrophysics, the Kavli Institute for Particle Astrophysics and Cosmology, the Korean Scientist Group, the Chinese Academy of Sciences (LAMOST), Los Alamos National Laboratory, the Max-Planck-Institute for Astronomy (MPIA), the Max-Planck-Institute for Astrophysics (MPA), New Mexico State University, Ohio State University, University of Pittsburgh, University of Portsmouth, Princeton University, the United States Naval Observatory, and the University of Washington.

REFERENCES

Abazajian, K. N., Adelman-McCarthy, J. K., Agüeros, M. A., et al. 2009, ApJS, 182, 543
Andrae, R., Kim, D.-W., & Bailer-Jones, C. A. L. 2013, A&A, 554, A137
Armitage, P. J., & Reynolds, C. S. 2003, MNRAS, 341, 1041
Armitage, P. J., Reynolds, C. S., & Chiang, J. 2001, ApJ, 548, 868
Arons, J. 1992, ApJ, 388, 561
Balbus, S. A., & Hawley, J. F. 1991, ApJ, 376, 214
Bauer, A., Baltay, C., Coppi, P., et al. 2009, ApJ, 696, 1241
Butler, N. R., & Bloom, J. S. 2011, AJ, 141, 93
Capellupo, D. M., Hamann, F., Shields, J. C., Rodríguez Hidalgo, P., & Barlow, T. A. 2011, MNRAS, 413, 908
Capellupo, D. M., Hamann, F., Shields, J. C., Rodríguez Hidalgo, P., & Barlow, T. A. 2012, MNRAS, 422, 3249

Cardelli, J. A., Clayton, G. C., & Mathis, J. S. 1989, ApJ, 345, 245
Cutri, R. M., Wisniewski, W. Z., Rieke, G. H., & Lebofsky, M. J. 1985, ApJ, 296, 423
Davis, S. W., Blaes, O. M., Hirose, S., & Krolik, J. H. 2009, ApJ, 703, 569
Davis, S. W., Woo, J.-H., & Blaes, O. M. 2007, ApJ, 668, 682
Dawson, K. S., Schlegel, D. J., Ahn, C. P., et al. 2013, AJ, 145, 10
Dexter, J., & Agol, E. 2011, ApJL, 727, L24
Filiz Ak, N., Brandt, W. N., Hall, P. B., et al. 2012, ApJ, 757, 114
Filiz Ak, N., Brandt, W. N., Hall, P. B., et al. 2013, ApJ, 777, 168
Frank, J., King, A., & Raine, D. J. 2002, Accretion Power in Astrophysics (Cambridge: Cambridge Univ. Press), 398
Gammie, C. F. 1998, MNRAS, 297, 929
Garcia, A., Sodré, L., Jablonski, F. J., & Terlevich, R. J. 1999, MNRAS, 309, 803
Gezari, S., Martin, D. C., Forster, K., et al. 2013, ApJ, 766, 60
Gibson, R. R., Brandt, W. N., Gallagher, S. C., Hewett, P. C., & Schneider, D. P. 2010, ApJ, 713, 220
Gibson, R. R., Brandt, W. N., Schneider, D. P., & Gallagher, S. C. 2008, ApJ, 675, 985
Gibson, R. R., Jiang, L., Brandt, W. N., et al. 2009, ApJ, 692, 758
Giveon, U., Maoz, D., Kaspi, S., Netzer, H., & Smith, P. S. 1999, MNRAS, 306, 637
Hirose, S., Krolik, J. H., & Blaes, O. 2009, ApJ, 691, 16
Hook, I. M., McMahon, R. G., Boyle, B. J., & Irwin, M. J. 1994, MNRAS, 268, 305
Ivezic, Z., Tyson, J. A., Acosta, E., et al. 2008, arXiv:0805.2366
Janiuk, A., & Misra, R. 2012, A&A, 540, A114
Jiang, Y.-F., Stone, J. M., & Davis, S. W. 2013, ApJ, 767, 148
Kelly, B. C., Bechtold, J., & Siemiginowska, A. 2009, ApJ, 698, 895
Kim, D.-W., Protopapas, P., Byun, Y.-I., et al. 2011, ApJ, 735, 68
Kozłowski, S., Kochanek, C. S., Udalski, A., et al. 2010, ApJ, 708, 927
Li, S.-L., & Cao, X. 2008, MNRAS, 387, L41
MacLeod, C. L., Brooks, K., Ivezić, Ž., et al. 2011, ApJ, 728, 26
MacLeod, C. L., Ivezić, Ž., Kochanek, C. S., et al. 2010, ApJ, 721, 1014
Meusinger, H., Hinze, A., & de Hoon, A. 2011, A&A, 525, A37
Meusinger, H., & Weiss, V. 2013, A&A, 560, A104
Noble, S. C., & Krolik, J. H. 2009, ApJ, 703, 964
Noble, S. C., Krolik, J. H., & Hawley, J. F. 2009, ApJ, 692, 411
Penna, R. F., McKinney, J. C., Narayan, R., et al. 2010, MNRAS, 408, 752
Pereyra, N. A., Vanden Berk, D. E., Turnshek, D. A., et al. 2006, ApJ, 642, 87
Reichard, T. A., Richards, G. T., Hall, P. B., et al. 2003, AJ, 126, 2594
Richards, G. T., Fan, X., Newberg, H. J., et al. 2002, AJ, 123, 2945
Ruan, J. J., Anderson, S. F., MacLeod, C. L., et al. 2012, ApJ, 760, 51
Sakata, Y., Morokuma, T., Minezaki, T., et al. 2011, ApJ, 731, 50
Schlegel, D. J., Finkbeiner, D. P., & Davis, M. 1998, ApJ, 500, 525
Schmidt, K. B., Marshall, P. J., Rix, H.-W., et al. 2010, ApJ, 714, 1194
Schmidt, K. B., Rix, H.-W., Shields, J. C., et al. 2012, ApJ, 744, 147 (SC12)
Schneider, D. P., Richards, G. T., Hall, P. B., et al. 2010, AJ, 139, 2360
Sesar, B., Ivezić, Ž., Lupton, R. H., et al. 2007, AJ, 134, 2236
Shakura, N. I., & Sunyaev, R. A. 1973, A&A, 24, 337
Shen, Y., Richards, G. T., Strauss, M. A., et al. 2011, ApJS, 194, 45
Stoughton, C., Lupton, R. H., Bernardi, M., et al. 2002, AJ, 123, 485
Trèvese, D., Kron, R. G., & Bunone, A. 2001, ApJ, 551, 103
Trèvese, D., & Vagnetti, F. 2002, ApJ, 564, 624
Turner, N. J., Blaes, O. M., Socrates, A., Begelman, M. C., & Davis, S. W. 2005, ApJ, 624, 267
Ulrich, M.-H., Maraschi, L., & Urry, C. M. 1997, ARA&A, 35, 445
Vanden Berk, D. E., Wilhite, B. C., Kron, R. G., et al. 2004, ApJ, 601, 692
Wilhite, B. C., Brunner, R. J., Grier, C. J., Schneider, D. P., & vanden Berk, D. E. 2008, MNRAS, 383, 1232
Wilhite, B. C., Vanden Berk, D. E., Kron, R. G., et al. 2005, ApJ, 633, 638 (WI05)
York, D. G., Adelman, J., Anderson, J. E., Jr., et al. 2000, AJ, 120, 1579
Zu, Y., Kochanek, C. S., Kozłowski, S., & Udalski, A. 2013, ApJ, 765, 106
Zuo, W., Wu, X.-B., Liu, Y.-Q., & Jiao, C.-L. 2012, ApJ, 758, 104